

Prolonging battery lifetime in various energy markets

Milán Attila Sőrés¹, Bálint Hartmann²

Department of Electric Power Engineering BME Faculty of Electrical Engineering and Informatics,
Egry J. str. 18., 1111, Budapest, Hungary.

¹soresm@edu.bme.hu, ²hartmann.balint@vik.bme.hu

Corresponding author:

Milán Attila Sőrés, soresm@edu.bme.hu

Hungary, 8200, Veszprém Kádártai street 31/2

Abstract: *Li-ion batteries are more and more common not only in the sector of e-mobility but their role is increasing in stationary storage as well. The possibilities of the use of these storages are various. In this paper, the authors were focused on the possibility of providing frequency reserve and other flexibility services for the grid. The paper focuses on the operation of a battery energy storage system and not the sizing of one. In the developed model the authors consider the profit from these services and their impact on the battery lifetime. With these two main factors, the operation of the battery system is compared in the case of different frequency reserve services and other market operations. Results show that battery energy storage systems have the potential for frequency reserve services in case of an optimized operation strategy. Simulation results also show that these optimized operation strategies can be different in different phases of the battery life. The presented model was developed under the EU Horizon 2020 programme in the OneNet project.*

Keywords: battery energy storage, stationary storage, electricity market operation, state-of-health

Nomenclature	
aFRR	Automatic Frequency Restoration Reserve
BESS	Battery Energy Storage System
CC	Constant Current
C _p	Specific heat capacity
CV	Constant Voltage
D	Degradation factor summary
d	Weighted degradation factor for each contributor
DAM	Day-ahead-Market
DoD	Depth-of-Discharge
DVA	Differential Voltage Analysis
EFC	Equivalent Full Cycle
E _{thr}	Energy throughput
EV	Electric Vehicle
FCR	Frequency Containment Reserves
LCO	Lithium Cobalt Oxide
LMFP	Lithium Manganese Iron Phosphate
LMNO	Lithium Manganese Nickel Oxide
m	mass
mFRR	Manual Frequency Restoration Reserve
n	nominal
n _j	period of the j-th service
NCA	Nickel Cobalt Aluminum
NMC	Nickel Manganese Cobalt
P	Profit

PV	Photovoltaic
pwr	Power
Q	Capacity
q	Heat
RES	Renewable Energy storage
S	Service
SEI	Solid electrolyte interface
SOC	State-of-Charge
SOH	State-of-Health
T	Temperature
TSO	Transmission System Operator
t	Time
U, u	Voltage
W	Weight function
δ	Degradation factor for each contributor

1. Introduction

Applications of battery energy storage systems (BESS) are rapidly growing worldwide. Battery usage can be grouped into three major application categories: e-mobility, stationary energy storage, and consumer electronics, including telecommunication devices. The global demand for stored energy was around 184 GWh in 2018, and 282 GWh in 2020, and exponential growth is estimated for the next decade reaching 2623 GWh in 2030 according to the Strategic Research Agenda for batteries by the European Commission [1], [2]. The driving force of this growth is mainly the electric vehicle (EV) sector, but increasing demand is observable for the stationary energy storage sector as well. For EVs the demand could be even higher as in 2021 the European Commission adopted the so-called ‘Fit for 55’ legislative package to further reduce net greenhouse gas emission [3]. From the energy production side, the spread of renewable energy sources (RES) means the necessity of increasing installed storage capacity. According to the Eurostat [4] the share of renewable energy production and consumption more than doubled between 2004 and 2019.

In this paper, the authors focus on stationary energy systems and their possibilities in the electricity market. On the electricity market, many different services can be sold. For a market player, there can be two different scenarios. The participant is new to the electricity market and the installation of a battery energy storage system is expected to make a profit. Or the market player already had a battery system, for example, next to a wind farm to balance the rapidly changing electricity production. In this second scenario, the battery system had been designed according to the specific requirement to align the wind farm production. In their paper authors of [5] show a case study of optimal BESS sizing for lowering wind farm operating costs. As new products are introduced to the electricity market it could be an option to provide extra services beyond the balancing of the owned wind farm. The main focus of our paper will be this second case when a BESS is already installed for some specific task, but as new services are introduced it is possible to allocate energy and operation time for them as well. The question for the battery system is how each type of service affects the lifetime of the battery. The first aspect usually is the profit of the services; however, it is also important to compare the services based on their effect on battery lifetime.

As mentioned earlier our goal is to compare different electricity market services, by which power profiles are meant from the battery point of view. Classic electricity market services for frequency regulations are FCR, aFRR, and mFRR or as previously called primary, secondary and tertiary reserves. These three services are to help restore grid frequency and the main difference between them is their duration, FCR is the first, and from 30 seconds aFRR replaces it with 5 minutes to provide the full reserve. Later from 12.5 minutes starts the mFRR supports the aFRR, if necessary. The authors of [6]

developed a method of the utilization of household-sized BESS for participating in FCR, aFRR, and also on the day-ahead market. In their paper Y. Hu et. al. examined option-based operation of the BESS, although their focus was on only FCR ancillary service from the system point of view [7].

The possible new services that are currently under research and development by the OneNet EU project will be a quarter-hour-based flexibility service – where ramp-up speed is not critical – traded on the day-ahead market.

In the following, the paper will be structured into the following sections. Section 1 is to observe and evaluate the main contributors and discuss their relations to battery aging. In Section 2 a methodology will be presented for determining the numerical value of these aging factors and the assigned weight to provide a comparison of the profiles. In this paper, the following two market services will be observed in terms of aging: FCR and aFRR. Besides them day-ahead-market (DAM) and intraday market are considered as well. [8] Section 3 presents an installed BESS from Hungary that will be used to evaluate the effects of the profiles. At the end of the paper, results are presented and discussed as well as future perspectives.

2. Contributors to degradation

In this section, the factors contributing to the aging process and their effects on each other are summarized, but the underlying causes of the exact aging phenomenon like SEI formation [9] or lithium plating [10] will not be discussed.

In literature, the aging of the battery is usually divided into two categories: calendar aging and cycling, as described by Broussely et al. [11] Calendar aging is the storage of the battery cells, while cycling is the intended operation. In this paper, we consider aging due to cycling rather than calendar aging, but the developed model considers longer times without charge or discharge (idle state) in case of high SOC. The following list contains the most important aging factors of a BESS according to the literature. Here, ordering in the list does not represent any information.

- Temperature
- C-rate (discharge/charge)
- SoC (initial, end)
- DoD
- FEC (full equivalent cycles)
- Idling time

Each element of the list is discussed in the next sections.

2.1. Temperature

Commercial lithium-ion batteries are usually possible to operate in a wide temperature range. The upper limit for safe operation is typically between 50 °C – 60 °C, while the lower limit is between -10 °C – 0 °C. Of course, these are just general values, the exact limits for a given battery type can differ from these. Despite the relatively wide range of use, continuous usage of the batteries in elevated or colder temperatures results in accelerated aging. Therefore, there is an optimal temperature is determined close to room temperature, in the range of 20 °C – 30 °C. This optimum for most of the cells is 23 °C or 25 °C, as shown in the examples [12], [13] and [14]. Allowed temperature limits are affected by the method of usage as well; there can be different safe temperature ranges for the charge, discharge, and storage, due to different electrochemical processes inside the cell.

2.1.1. High Temperatures

For higher temperatures (25 °C and above) Dubarry et. al. [15] found that two types of prismatic LFP cells cycled with C/2 for 100 times, and lost 37% of their initial capacity. Feng et. al. [16] examined the aging mechanisms, of LCO chemistry cells, at 25 °C, 35 °C, 45°C, and 55 °C with constant 1C discharge. They found that after 250 discharge cycles the capacity decrease was 4.22%, 6.57%, 8.74%, and 13.24% respectively. In their study Zhang et al. [17] studied the storage of cells at elevated temperatures and compared the results to non-stored, only cycled battery cells. At 25 °C the stored and non-stored cells yield similar results, between 5 - 6 % capacity loss after 100 cycles. Cells stored at 60 °C lost almost 10 % of their capacity, while for 70 °C the loss was around 17 %. Authors of [18] investigated NMC-111 chemistry cells at 40 °C and 60 °C with different discharge current rates from 0.1C to 1C. Capacity loss at 40 °C was between 1 – 3 % for 100 cycles, while for 60 °C the results are between 2 – 6 %. Gilbert et al. in [19] examined NMC-532 chemistry cells, in the voltage range from 3V to 4.4V, which is above the usual 4.2V voltage cutoff limit. They measured both charge and discharge capacity fade at 30 °C, the results were 10.8 % and 18.9 % respectively. Similar elevated cut-off voltage limit cycling was done by Buchberger et al. [20], though they investigated cycling results in the case of 4.6V for NMC-111 cells. The results were compared to cycling at room temperature and 60°C both with 1C. Capacity fades for 25 °C at around 2.3 % for 60°C at around 28% and the worst result for 100 cycles with 38% capacity loss is the elevated cut-off voltage. In 2014, Ziv et. al. [21] examined three chemistries (LMFP, HC-NMC, and LMNO) at 30 °C and 60 °C. The capacity loss at 30°C varied between 21 – 46 %, and between 34 and 60 % at 60 °C.

The above-presented results show very different results, presumably because of the different chemistries, and different aging methods (cycling current or storage). Because of these reasons in the further sections, only NMC-type cells will be considered, as later the modeled battery system is made up of NMC chemistry cells. In their work, Waldmann et al. [22] investigated a range of temperatures starting from -20 °C and ending at 70 °C. Their results are exceptionally useful as results of high and low-temperature aging can be observed. According to their work lower temperatures have a higher aging effect on the cells making the SOH (State-of-Health) decrease as a function of temperature asymmetrical. Researches on degradation are rather rare, although in [23] the authors compared different electrolytes at 80 °C, in our case for safety reasons [24], [25] temperatures above 70 °C will be avoided. Jalkanen et al. [26] examined commercially available Kokam 40Ah cells. In their work, they observed cell cycling at room temperature, 45 °C, and 65 °C climate chamber. While cells cycled at elevated temperature lost their capacity steadily, for room temperature cells, this monotonous capacity decrease started roughly after 500 full cycles. That may indicate that at room temperature the full-equivalent cycles affect capacity fade, however, this effect was not observable in the case of 45 °C and 65 °C.

2.1.2. Low Temperatures

In the previous section study considering lower temperatures [22] was already mentioned, however, it is important to have more data on this topic as well. Here lower temperatures mean that lower than the optimal 25 °C. Wu et. al. [27] conducted their cyclic measurements at -10 °C with different C-rates. To get comparable results they used reference measurements at 25 °C. Capacity fade was between 5 and 20% depending on the discharge current at the 100th cycle. In 2017 Matadi et al. [28] found significant capacity loss for a commercial 16Ah NMC cell. Cells with full cycles, in the allowed range of 2.7 V to 4.2 V lost around 75% of their initial capacity. That is probably due to on one hand the high upper voltage limit, on the other hand, the charging current of the constant current (CC) phase was 1C as opposed to the manufacturer's recommendation of 0.3C between 0 °C and 10 °C. Friesen et al. [29] similar results for a 2.2 Ah NMC-532 cell, as the end of life limit, was set to 70% (lower than the usual automotive limit, 80%) the cells reached this limit in 50 cycles with 1C load. It is important to note that, the cells were initially unable to provide 2.2Ah at this temperature. Their initial capacity was around 72% of the nominal at the start. In 2017 authors of [30] cycled NMC-111 chemistry cells at -10°C, with various C-rates. Although only 40 cycles were performed at this low temperature the capacity loss is still remarkable, for 1C it is more than 50% of the original capacity. Wu et al. [31]

compared the aging mechanism of NCA-type cells, at three different temperatures, 10 °C, 25 °C, and 40 °C. The results of 10 °C cyclings were only a bit higher than the 25 °C measurements.

In conclusion in the above describe literature three main points can be highlighted:

- The optimal temperature of commercial Li-ion cells is around 25 °C.
- Temperature effects on aging is asymmetrical.
- Temperatures below -20 °C or above 70 °C should not be considered, either for safety or initial capacity loss concerns.

2.2. C-Rate

In this subsection, the aging effect of different C-rates will be discussed. The C-rate of a battery represents a current, though the C-rate itself has no unit. C-rate is the current with which the battery is charged or discharged relative to the reference current, or the nominal capacity. [32] In general, it can be concluded that the higher the C-rate, the higher the degradation of the battery. It is always limited both for continuous and short time cases. There are two different types of cells, the so-called “power” and “energy” cells. The “power” cells as their name suggest are optimized to deliver higher power, which means higher discharge current. In some cases, it can be more than 10C. High power requirements are typical for e-mobility applications electric cars or aviation. [33]

For stationary storage applications, however, “energy” type cells are used with lower allowed C-rates, 1C or even less. In these cases, space and mass mean no or less restriction compared to e-mobility. From commercial datasheets, a general rule can be considered as the maximum C-rate for charging and discharging are different. It is possible of course to find cells, that have the same limit for charge and discharge, but only lower C-rate cells have this feature. It is almost impossible to find a cell, that can be discharged with 10C, and the charging C-rate is in this range as well. Also, fast charging contributes to the aging phenomenon, especially at low temperatures, one of the main challenges of today’s e-mobility industry.

In case we investigate literature, several publications are examined the effects of C-rate. In our paper selected results from them will be presented. In 2019 Saxena et al. [34] examined several commercially available cells with different C-rates from 0.2C to 2C. Although the test results showed some variance, they managed to create a model to estimate the results of low C-rate cycling from high C-rate cycling measurements. Measurements were concluded at 37 °C which as previously shown is a slightly elevated value. From their work, it can be seen that low and very low C-rates (below 0.2C) have little contribution to aging, while 0.5C, 1C, and 2C caused significant capacity fade over the cycling. Ning et al. [35] cycled 1.4 Ah capacity 18650 size cells with 1, 2, and 3C-rates through 300 cycles. Their results show that cells cycled with higher C-rates aged faster, and also their internal resistance increased faster. Murashko et al. [36] cycled different chemistry cells with different charging C-rates at 45 °C until 15% capacity loss. In their work, the authors developed a DVA-based method, for determining aging mechanisms in the Li-ion cells. In their study Choi et al. [37] investigated the effect of C-rate in both charging and discharging directions in the range of 1C to 2C. From their work, the higher current adversely affects the capacity of the examined cell.

2.3. EFC

Equivalent full cycles (or in some papers FEC – full equivalent cycles) are the energy throughput of the battery relative to the nominal energy. [38] It can be calculated by a simple equation (1) as in the authors of [39] presented:

$$N_{EFC} = \frac{E_{thr}}{2 \cdot U_n \cdot Q_n} \quad (1)$$

It is an important value because battery manufacturers usually give a maximum value under optimal operation conditions, so it gives an operational limit.

2.4. SOC

The state-of-charge of a battery affects the cyclic performance in three different ways. At first, the SOC level itself has a contribution to aging, this is mainly studied in calendar aging examinations. In 2014 Ecker et al. [40] did comprehensive research on the topic with various SOC’s for storage. In general, the higher SOC contributes to more elevated aging. The second way SOC affects aging is the used SOC

range. In their study the authors compared different SOC ranges for $\Delta\text{SOC} = 100\%$ (full discharge) to $\Delta\text{SOC} = 5\%$, symmetrical to 50% SOC. In the first case, the cells could provide around 440 full equivalent cycles, while in the second the number increased to 8500 full equivalent cycles until the capacity reached 80%. It must be noted however that the second result, is only a linear interpolation, the presented cycle number did not reach 4000. On the contrary Harlow et al. [41] provided even better results for battery aging, though, their research was done not on commercially available cells, but on cells that are modified.

3. Evaluation of degradation

There are several articles regarding battery sizing. Mostly these articles consider a single or few purposes for the battery. In their article [42], the authors listed the possibilities for these applications. Sizing for an application is for example [43] where the authors researched the sizing and optimal operation of a BESS with a PV system. In the primary goal of BSS sizing is frequency regulation. In terms of operation of the battery sometimes the placement of the BESS is considered as in [44]. Another example of a dedicated reason for sizing a battery system is where [45] the energy storage system supports dynamic inertia [46]. These articles usually neglect battery aging or implement a simple aging model. Of course, more detailed models exist as well, but the used parameters of these models can be obtained with several time-consuming measurements [47].

There is multiple literature for BESS strategies as well, but usually they take into consideration only some of the above-mentioned aging contributors. As an example, in [7] the authors take into consideration only FEC and DoD, while in [48] and [49] only SoC and DoD play significant roles. For different applications there can be found different developed strategies, but these are focusing only on some of the possible battery functions, like only FCR or aFRR, or other non-system related operation scenarios like peak-shaving or energy arbitrage as in [50] and [51], respectively.

In our paper, we focus on a BESS that has been already built for some specific reason (frequency regulation, inertia support, operating with renewables, etc.). Therefore, battery sizing questions are not in the scope of this article. So, the main parameters of the investigated system, such as cell configuration or cooling method, are fixed and cannot be changed. This article focuses on the operation of the battery in a scenario where the battery is capable of providing different services for the electricity market. These can be services that are already possible to provide or new services that are not introduced so far. In this scenario, the different services are present as power vs. time functions, in this article called profiles. As the battery parameters are fixed, it is possible to evaluate different profiles regarding their possible effect on battery aging. All profiles have different characteristics contributing to battery aging, the most important ones are summarized in the previous section. These will be called degradation factors and will be denoted by d_{ij} , where i stands for the i -th degradation factor, and j for the j -th profile. The degradation factors for each profile can then be summarized into one cumulated degradation factor (2) characteristic for the profile.

$$D_j = \sum_i d_{ij} \quad (2)$$

The optimization task is to minimize the degradation for a given period (3) with the calculation of the number (n_j) of these profiles that can be executed.

$$\min(\sum_j (D_j \cdot n_j)) \quad (3)$$

Note that n_j always has an upper limit either because of the given period or the battery state limits, for example, the actual SOC. The obvious solution for this problem would be if each n value would be zero, therefore, and for natural market player reasons another equation is required that ensures the maximal profit. Similarly, to the previous degradation factors, a profit (P_j) is assigned to each service. The profit is maximized with equation 4.

$$\max(\sum_j (P_j \cdot n_j)) \quad (4)$$

3.1. Degradation factors

These factors are calculated to form the profiles and the actual states of the battery and will be weighted based on the information from the literature review. The general formulation of the degradation factors will be:

$$d_{ij} = W(\delta_{ij}) \quad (5)$$

Where δ_{ij} is the contribution of each profile to each degradation factor, while W is a weight function.

For battery states the SOC, T, and the actual cycle number are considered EFC act. In this section, the calculation of the degradation factors d_{ij} is presented. They are the same that were detailed in Section 1, but not necessarily in the same order.

3.1.1. C-rate

The first factor, denoted with d_{1j} is the C-rate, more specifically the maximum of the C-rate, as the profile is a function of time, so can be the C-rate. For a given $P(t)$ function the C-rate can be expressed as:

$$c_{rate}(t) = \frac{pwr(t)}{u(t)} \cdot \frac{1}{Q_n} \quad (6)$$

Although $p(t)$ is given and Q_n is known, $u(t)$ is the battery response for the applied $p(t)$. To determine $u(t)$ we would need some battery model. Models would require measurement data and would slow down the algorithm therefore we will approximate the result, with U_n , nominal battery voltage (7). Note that our goal is not to exactly calculate battery response, only to compare the possible profiles with each other.

$$c_{rate}(t) = \frac{pwr(t)}{U_n} \cdot \frac{1}{Q_n} \quad (7)$$

For eq. 7. d_{1j} factor can be calculated as:

$$\delta_{1j} = \max(|c_{rate}(t)|) \quad (8)$$

The absolute value of the C-rate is necessary as it is possible to change power direction during a profile, which means change from charge to discharge. For example, in a case where the battery provides frequency reserve, after the activation, it shall be recharged.

3.1.2. SoC and DoD

The second and third factors are related to the state of charge. The state of charge can be calculated simply with the coulomb counting method. The current will be estimated similarly to the C-rate case with U_n . It has to be noted that our definition of the SOC range is analogous to the definition of depth-of-discharge (DoD), which is also widely used.

$$\delta_{2j} = \Delta SOC = \frac{1}{Q_n} \cdot \int \frac{pwr(t)}{U_n} dt \quad (9)$$

In this case, δ_{2j} is equal to ΔSOC . Not only the range of the SOC is important, but the remaining SOC as well. Partly because it has some effect on the next profile, but also because the effects in shown in calendar aging.

$$\delta_{3j} = SOC_{rem} = SOC_{init} - \Delta SOC \quad (10)$$

Where SOC_{rem} is the remaining SOC, and SOC_{init} stands for initial SOC. Then δ_{3j} will be equal to SOC_{rem} .

3.1.3. EFC

Equivalent full cycles give information on how many cycles our BESS is capable of. Eq. 1 shows the calculation method for EFC, and eq. 11 shows the next factor.

$$\delta_{4j} = \frac{1}{Lifecycle_n} \frac{1}{2 \cdot Q_n \cdot U_n} \cdot \int pwr(t) dt \quad (11)$$

3.1.4. Temperature

In the case of the temperature, a simplified model is required. Although the cell temperature is indeed connected both to the I_{RMS} value and the energy throughput, which is much easier to calculate, weighting these values would be rather hard since temperature effects on aging are included directly in the literature review.

$$\delta_{5j} = T_{end}(pwr(t)) \quad (12)$$

Where T_{end} is the temperature that the battery reaches at the end of the profile. Temperature is calculated from the generated heat from the power loss of the cell, eq.13.

$$m \cdot C_p \frac{\partial T}{\partial t} = q_{diss} - q_{conv} \quad (13)$$

During the years several models have been developed and published, this basic equation is from papers [52] and [53]. In our model, we assumed free air convection, and the model neglects radiative heat transfer. Heat capacity is estimated by the value of aluminum. The heat generated by side reactions is also neglected. This is a generally accepted thermal model for the simple calculation of a battery system.

3.2 Weights

In this section, the authors discuss the used weights for each degradation factor, based on the measurement results presented in the first part, the literature review. In this section the lower-case j notes, that indicates the index of the profile is not shown in the equations. These weights can be considered general, as the above-mentioned degradation contributors may have some differences in case of different Li-ion battery chemistries. For the comparison of service cause degradation this general model is considered appropriate, in case of a new battery design a more detailed battery model might be necessary. In our simulation an NMC chemistry-based BESS was used, detailed parameters are discussed in section 4.2.

3.2.1 C-rate

Based on the reviewed literature in the first section, it can be stated that increasing the discharge / charge current will lead to more and more increasing SOH fade. There is a manufacturer-allowed current limit for both charge and discharge, that represents the maximum of the weighting function. The proposed weight function is a sigmoid function namely the logistic function, eq. 14.

$$W_{C-rate}(\delta_1) = \frac{L_C}{1 + \exp[-k_C \cdot (\delta_1 - x_{0,C})]} \quad (14)$$

The maximum of the function (L_C) is 25, the steepness coefficient k_C is 20, and the midpoint ($x_{0,C}$) is set to be 0.5.

3.2.2 SOC window

The SOC window represents the difference between the beginning and end SOC of a given profile. Capacity fade is highly dependent on this window. An exponential weight function is proposed based on results from [40].

$$W_{\Delta SOC}(\delta_2) = A_{\Delta} \exp(B_{\Delta} \cdot \delta_2) \quad (15)$$

Coefficients A_{Δ} and B_{Δ} are 1.942 and 0.0554 respectively.

3.2.3. Remaining SOC

The weight for the remaining SOC is calculated based on the capacity fade of calendar aging results. The reason for this calculation is to observe how much the SOH would be affected if the battery would remain in that state. In general, 0% remaining SOC means insignificant aging, while 100% SOC would

cause more capacity loss than low C-rate cycling [40]. The proposed weight function is eq.16., based on those two values.

$$W_{SOCrem}(\delta_3) = A_r \exp(B_r \cdot \delta_3) \quad (16)$$

Coefficients A_r and B_r are estimated to be 1.1426 and 0.323 respectively.

3.2.4. EFC

For the equivalent full cycle, the weight should show that at the beginning of life the number of equivalent cycles is almost insignificant, as cells nowadays could provide several hundred or even some thousand cycles. The factors should be more and more important as the cells approach the theoretical cycle life limit. Because of these reasons a sigmoid type function, namely, the logistic function is chosen eq. 17, with coefficients that resemble the rise of the degradation factor value from around 80%.

$$W_{ECF}(\delta_4) = \frac{L_{ECF}}{1 + \exp[-k_{ECF} \cdot (\delta_4 - x_{0,ECF})]} \quad (17)$$

The maximum of the function (L_C) is 25, the steepness coefficient k_c is 30, and the midpoint ($x_{0,c}$) is set to be 0.5.

3.2.5. Temperature

Weighting the temperature value will be separated into two regions by the optimal operating temperature, since its asymmetrical behavior. Unfortunately, most papers did not examine the whole operating temperature range by for example 5 °C steps, usually, only two or three different measurements are given. Some exemptions are [16], [22], and [26]. Although it is always possible to linearly interpolate the measured values, the results show that an exponential function could yield better estimation results, in terms of R2 values. Therefore, for temperatures, an exponential weight function is used. To determine the parameters for this function, the other reviewed data is also included, in the following way. For each measurement, the coefficients of the exponential functions are estimated, and after that, the estimated capacity loss from these functions is averaged. From these averaged results, the weight function coefficients are estimated. The weight equation for $T_{end} \geq 25$ °C eq. 18 is given:

$$W_{T,high}(\delta_5) = A_{high} \cdot \exp(B_{high} \cdot \delta_5) \quad (18)$$

where δ_5 is the degradation factor, A_{high} and B_{high} are the coefficients of the exponential function with values of 5.0398 and 0.021 respectively. For low ($T_{end} < 25$ °C) the equations form is the same, eq. 19, only coefficients are changed to A_{low} and B_{low} , 42.6619 and -0.0717. These coefficients are estimated with the help of [22].

$$W_{T,low}(\delta_5) = A_{low} \cdot \exp(B_{low} \cdot \delta_5) \quad (19)$$

In the end of this sections Table I. gives a summary of the coefficients for each weight equation.

Table I.

Coefficient	Corresponding factor	Value
L_C	C-rate	25
k_C	C-rate	20
$x_{0,C}$	C-rate	0.5
A_Δ	SOC range	1.942
B_Δ	SOC range	0.0554
A_r	remaining SOC	1.1426
B_r	remaining SOC	0.0323
L_{ECF}	ECF	25
k_{ECF}	ECF	30
$x_{0,ECF}$	ECF	0.85
A_{high}	Temperature	5.0398

B_{high}	Temperature	0.021
A_{low}	Temperature	42.6619
B_{low}	Temperature	-0.0717

4. Simulation setup

4.1. Profiles and profits

In our research, we used six power profiles, to evaluate the developed algorithm. The profiles are denoted with S_j , where S refers to the service (to avoid confusion with profit or power), and j is the index. Fig. 1 shows the defined profiles. The objective of the paper is to evaluate these services and present a framework in which newly defined services can be compared based on degradation. When a battery owner contracts to mandatorily provide a service, and pays significant fines in case the system fails to deliver. Therefore, the power profile cannot be altered, even if the battery aging status would require due to capacity loss, or resistance increase.

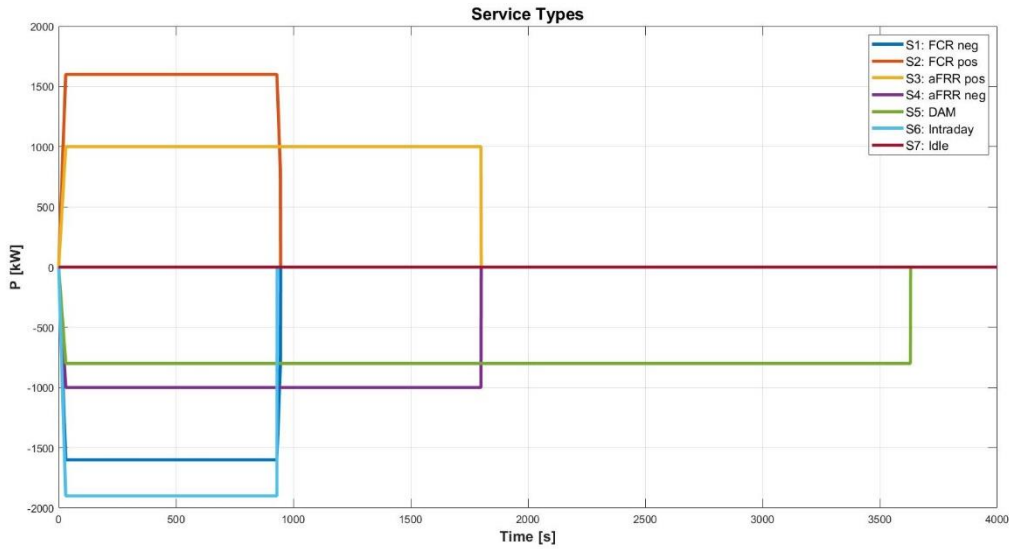


Fig. 1. Power profiles

As Fig. 1. shows the power of the profiles is in kW, and the time is in seconds. From the electrical market point of view, the power is measured at 15 minutes intervals (which refers to typical settlement periods). The negative power indicates charging the battery, or from a grid viewpoint, the BESS is a consumer, while positive power means discharging the battery, or it acts as a producer. The profiles tend to represent real scenarios, S1, S2 and S6 are short time, high power consumption or production, while S3, S4, and S5 represent a longer use interval with lower power. It shall be noted that S1 and S2 are symmetrical to the P-axis, just like S3 and S4. To calculate the profit there are many possibilities. The simplest version is to assign a profit value to each profile, there no calculation is required. The second possibility would be to calculate electrical energy in both charge and discharge directions from the profile, then assign a profit value to these signed energy values. This would represent better the market situation. A more complex method would be to dynamically change the profit, based on the actual state of the network. In our study, the fixed energy-based profit calculation is used Table II. shows the calculated energy values and the assigned prices. Of the six load profiles, four are discharges and two are charges of the BESS. Charging or discharging to the initial value of the battery systems is considered to be the same for all cases therefore their impact is neglected when comparing the services.

Table II.

Profile	Represented Service	Energy [MWh]	Energy Price [€/MWh]	Reserve Price [€/MWh]
S1	FCR	0.4113	0.0	42.6
S2				
S3	aFRR	0.5	409.0	37.8
S4			274.5	31.7
S5	DAM	0.8067	40	0.0
S6	Intraday trading	0.4908	20	0.0

4.1.1. Idle Profile

Another “service” is defined to represent those periods where no other service is active. We can consider the previous six services as profit-generating and this one as no profit generation. But it must be emphasized that aging in the BESS happens without providing energy, it is usually noted as calendar aging., therefore degradation factor has to be calculated for this as well.

4.2. Battery for the case study

The battery on which we examined our algorithm is an installed stationary storage battery in Hungary, Földeák substation. The BESS system is made of prismatic Samsung NMC cells. Table III. contains the relevant parameters of the battery system. [54]

Table III.

Parameter	Unit	Value
Voltage	[V]	730
Capacity	[Ah]	2256
Energy	[kWh]	1644
Peak Power rate	[-]	1.2
Modul weight	[kg]	54
Cell R_{DC}	[mOhm]	0.75
Optimal Temperature	[°C]	23
Nominal cycles	[-]	8000

4.3 Simulation algorithm

For the simulation, there are two possible methods and both are implemented. Both simulation processes can be divided into two separate parts. In the first part, the simulation calculates the accumulated degradation factors for each service based on the actual power profile and the given initial conditions (e.g. T, SOC). The second part of the simulation solves a linear programming problem, for the optimal number of n_j in a given period.

4.3.1 Online simulation

In this case, the initial conditions are the results of the previous service, therefore the degradation factors change from profile to profile. The linear programming problem is simplified to a choice between the lowest degradation factor and the highest profit services. In this case, no planning is included the whole period shall be simulated. There can not be a case where the battery is not capable of providing services,

as the degradation factors would prevent this problem. With a short example, if a battery starts from 50% SOC and the profit and degradation factors would show that a discharge service (Service 1) is the best that reduces the SOC by 20% and the cumulative degradation factor is $D_{1,1}$ and the profit is $P_{1,1}$ (here the first number represents, the number of the service, and the second is the simulation number). In the next simulation $D_{1,2} > D_{1,1}$ because of the remaining SOC value, and $P_{1,1} = P_{1,2}$. In this case, the chosen profile may be a profile with lower profit, but also a lower degradation factor.

The longest power profile is 1 hours long, considering additional 1 hour resting period for the battery the whole simulation period will be divided into 2 hours. In this case in one day 12 services are realizable, and in one week 84. This is only for simplification reasons. In Fig. 2. The flow chart of the online simulation is shown.

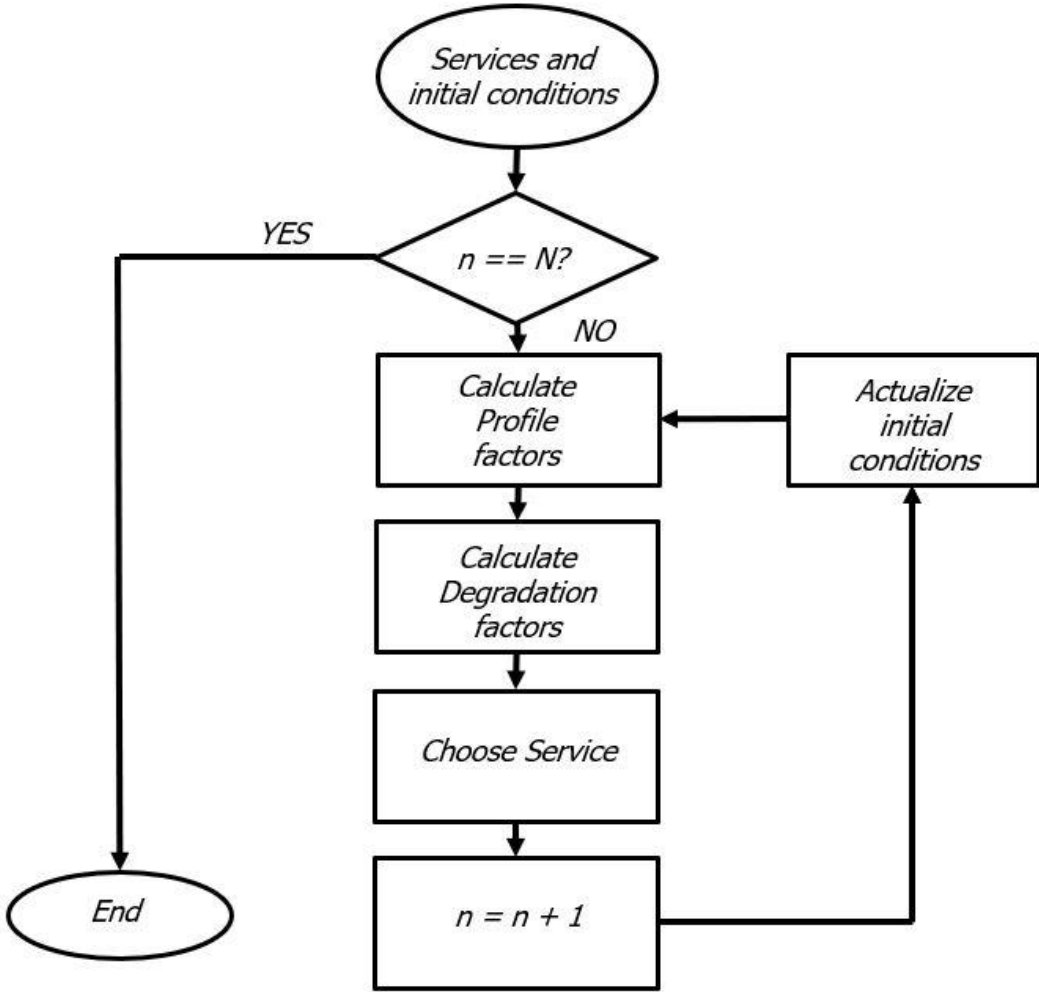


Fig. 2. Online simulation algorithm

4.3.2. Offline simulation

In this case, the initial conditions are the results of the previous service, therefore the degradation factors change from profile to profile. The linear programming problem is simplified to a choice between the lowest degradation factor and the highest profit services. In this case, no planning is included the whole period shall be simulated. There cannot be a case where the battery is not capable of providing services. In offline, or planning mode the degradation factors are calculated only once. That assumes each simulation starts from the same initial conditions. For that, the services will be changed, in a way that each service longs for 4 hours. In the additional time for the profile, the battery is assumed to be capable to return to the initial state. (Charge or discharge to the initial SOC, and cool back to the optimal temperature). During this period, it is possible to charge / discharge a battery with a low current that affects the aging minimally. In this way EFC is maintained constant during the period, for shorter

periods, a week does not mean a great error. Of course, the aging will appear in the next simulations as the EFC is calculated continuously. The initial value can be changed for the next simulation, for example simulating the next week. Fig. 3. shows the flowchart of the offline simulation.

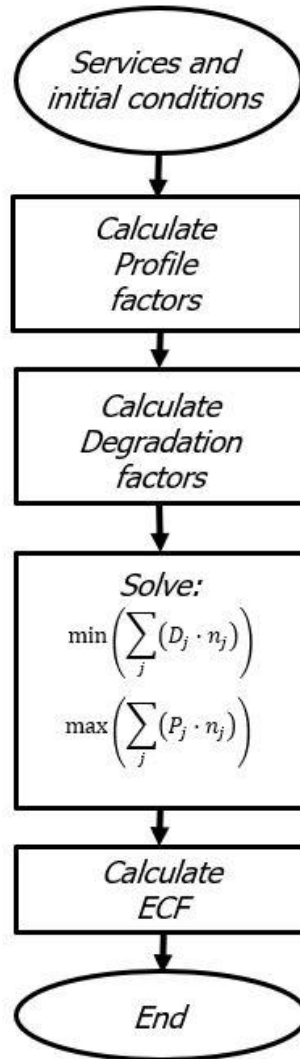


Fig. 3. Offline simulation algorithm

4.4. Optimization methods

In both online and offline cases, there is a step where there is a decision to make which profile will be selected. On the diagrams, it is either shown as *select profile* or *solve the equations*. For that different possibilities will be shown in this section. They will be different in what is the property that is more important for us. For this, the original set of equations will be slightly modified. In Eq. 4 it is stated that we want to maximize the profit, therefore it is a maximization objective. However, it can be changed to a minimization task. Since each defined service has a profit value it is possible to calculate a theoretical maximum profit. Then subtracting the actual scenario profit gives a type of difference between theoretical and actual profit, eq. 20.

$$P_{diff,j} = P_{max} - P_j \quad (20)$$

where P_{max} is the theoretical profit maximum, P_j is the actual profit of the j^{th} service, and $P_{diff,j}$ is their difference. Now the minimum of eq. 21 is provided by the same service as for eq. 4.

$$\min(\sum_j(P_{diff,j} \cdot n_j)) \quad (21)$$

4.4.1. Minimal aging and maximum profit

With eq. 3 and eq. 21 we have two terms to be minimized. One of the possible strategies is to calculate the internal multiplication for each combination of services as in eq. 22 and 23. There is a third equation for n , the time horizon for which the profile selection is made. For online mode $n = 1$, for offline mode, it is arbitrary eq. 24.

$$D_k = \sum_j (D_j \cdot n_j) \quad (22)$$

$$P_k = \sum_j (P_{diff,j} \cdot n_j) \quad (23)$$

$$N = \sum_j n_j \quad (24)$$

where index k refers to the combination. Then select the combination with the minimum of the sum of D_k and P_k .

4.4.2. Minimal aging, then maximum profit

To maximize the lifetime of the BESS it is a better approach to select a number from the least aging contribution combinations, for example, the least 10 and chose the one that offers the maximum profit. Generally, the set of equations 21, 22, and 23 is not changed only the that we reduce the cases based on D_k values to the best 10 and the chose the best based on P_k . Note that the percentage value is completely arbitrary.

4.4.3. Maximum profit, with minimal aging

The same as the previous one, with the difference that the selected roles are changed between D_k and P_k . First, select the highest 10 profit combination, then chose that gives the least aging.

4.4.4. Number of combinations

For a given period the number of possible services is different. In this paper, we consider the period in days. For DAM and Intraday it is set that one is possible in one, so in one day either a DAM or Intraday service can be provided. However, for FCR and FRR services the main value is the availability for longer periods. For FCR it will be set that, one FCR consumes 30 days, one day in which the service is provided, and 29 days in idle mode. This is based on the provided frequency data by Hungarian TSO: MAVIR. [55] Based on their frequency measurements roughly 1 frequency limit violation occurs per month. For aFRR, the data is based on data provided by Hungarian Energy and Public Utility Regulatory Authority. Data from Monthly Market Monitoring Report: Electricity between 2019 September and 2022 March are used for the statistics. [56] In the case of aFRR, the merit order plays a significant role in activation, therefore we considered the activation is most likely if the activated aFRR energy is greater than or equal to 50 MW. Days were counted with this power criteria. The authority provides these data only from 2019.09, hence the start of the period. Unfortunately, the data is distorted by the COVID pandemic, 11 months from the total 31 were affected by COVID measures, which is around 1/3 of the whole period. Because of this uncertainty the results are multiplied by 0.65 (11 over 31) The results are the average activation for positive aFRR is 3.2 days / month, while for negative aFRR is 2.9 days / month, therefore it will be considered 3 days / month for simplification. In our simulation aFRR will consume a maximum of 3 days for service providing and a minimum of 27 days in idle mode.

5. Results and Discussion

In this section, top 10 results from different optimization strategies are presented for a 10-day time period. Table IV. shows the results for aging and profit optimization. The rows contain each service combination and result. The numbers below each service is the number of the service performed. Column titled D [%] contains the relative degradation compared to the best from the chosen set. Profit [€] is the accumulated profit for the service combination.

Table IV. - Minimal aging, then maximum profit

Nr.	FCR	aFRR_pos	aFRR_neg	DAM	Intraday	Idle	D [%]	Profit [€]
1.	0	3	0	0	0	27	4.532	1180.5
2.	0	2	1	0	0	27	2.266	1082.7
3.	0	2	0	0	10	18	49.778	1179.7
4.	0	1	2	0	0	27	0	984.9
5.	0	2	0	1	9	18	50.439	1172.7
6.	0	2	0	2	8	18	51.090	1165.7
7.	0	2	0	3	7	18	51.760	1158.7
8.	0	2	0	4	6	18	52.421	1151.7
9.	0	2	0	5	5	18	53.092	1144.7
10.	0	2	0	6	4	18	53.75	1137.7

According to table IV. positive direction aFRR service dominates the best combinations. These strategies can be provided best at the beginning of life when degradation may be less important. This is true because their degradation factors are lower than the day-ahead market and intraday market. Their profit is the highest only in case they are activated in the period, as the number indicates, then besides the reserve price, the activation price is also paid to the operator. With DAM or intraday profiles, the degradation increases significantly, this is due to the fact that the idle period reduces significantly, which offers the best degradation numbers for the given initial conditions. Note that these initial conditions (SOC = 50% and T = 25 °C) cause relatively low calendar aging, it would be different with other setups, higher initial SOC for example. Operation with DAM or intraday increases aging by circa 50%. In terms of profit, the difference is not so significant, it is around 200 €. Interestingly FCR is not an optimal service in this case due to the low profit associated with it, although its degradation factor would be smaller. In this case, from all the possible combinations, the fourth row contains the minimal aging of the battery system. Note that here the system would age as well, but all other combinations accelerate the aging phenomenon more, most of them by around 50%. In physical quantities that could mean that if the capacity of the battery would be decreased by 1% as an example during the 4. scenario, then it would lose 1.5% in the case of the 5. column scenario. Of course, this is a simplified example, for the exact aging in the case of the 4. scenario a more detailed battery model would be required, which was not in our scope.

Table V. shows the results for aging optimization, and Table VI. shows the results for profit optimization.

Table V. - Minimal aging and maximum profit

Nr.	FCR	aFRR_pos	aFRR_neg	DAM	Intraday	Idle	D [%]	Profit [€]
1.	1	0	0	0	0	29	0	525.6
2.	0	0	3	0	0	27	8.52	887.1
3.	0	1	2	0	0	27	11.03	984.9
4.	0	2	1	0	0	27	13.56	1082.7
5.	0	3	0	0	0	27	16.07	1180.5
6.	0	0	2	0	10	18	61.28	984.1
7.	0	0	2	1	9	18	62.01	977.1
8.	0	0	2	2	8	18	62.75	970.1

9.	0	0	2	3	7	18	63.48	963.1
10.	0	1	1	0	10	18	63.79	1081.9

In case aging is our priority, possibly towards the end of life, FCR service becomes a better choice; as discussed previously it has a lower degradation factor, compared to aFRR, DAM, and Intraday services. However, FCR service offers a relatively low profit, around 50% lower compared to the best alternatives. In this case, the order follows the degradation factor order for the services, as the base is the first column scenario. The basic rule of degradation is the same as mentioned in the previous case. This operation strategy would be useful when the battery system is in an aged state (but nonlinear rapid capacity is not yet observed). As an example, The EOL of the battery is determined at 60% of the initial capacity, and the remaining capacity in the battery is 65%. In this example, if the first scenario would cause 1% capacity loss then it can be offered five-time, while 10. the scenario only twice. In this case, the profit would be higher with the 1. scenario. Note one important thing however, the direct comparison between the tables is not possible, because rows may contain completely different service combinations, and baselines are not the same.

Table VI. Maximum profit, with minimal aging

Nr.	FCR	aFRR_pos	aFRR_neg	DAM	Intraday	Idle	D [%]	Profit [€]
1.	0	3	0	0	0	27	0	1180.5
2.	0	2	0	0	10	18	43.286	1179.7
3.	0	1	0	0	20	9	86.563	1178.9
4.	0	0	0	0	30	0	129.855	1178.1
5.	0	2	0	1	9	18	43.925	1172.7
6.	0	1	0	1	19	9	87.22	1171.9
7.	0	0	0	1	29	0	130.484	1171.1
8.	0	2	0	2	8	18	44.554	1165.7
9.	0	1	0	2	18	9	87.831	1164.9
10.	0	0	0	2	28	0	131.123	1164.1

According to maximizing to profit optimization, the best possibility is positive aFRR again, with both reserve and activation energy prices. This strategy can be best suited for a battery at the beginning or mid of its life. However, the other close-to-optimal profit choices can increase the degradation of the battery dramatically, some of them would age twice as fast as the others, without any significant profit increase. It is interesting to observe that degradation can vary significantly between each case, and compared to the other tables, achievable profit is not so much more than the profit-oriented case. For these scenarios a more detailed battery model could be helpful for decision making.

Note that in the aging optimization strategy the service combinations are ordered by D [%], while in the case of profit optimization it is ordered by P [€].

6. Conclusion

In a summary, it can be stated based on Table IV. and VI. that considering battery aging problems has a significant role in operation management. Without it the operation strategy may result in much faster aging, yielding no significant income difference. In this paper the authors presented three simple method for operation strategy and assigned to them possible life phases of the battery system. Results show that batteries have a place among other system reserve providers not only based on their technological features but from an economic point of view as well. Scope of further work with this simulation framework could consider different initial conditions, the difference in results if activation for reserve

services did not happen and other more sophisticated operation strategies, and if there are any, new services of course. This battery-operated model will be used in the OneNet project by WP 10 Hungarian demonstration for testing flexibility services.

Declaration of competing interest

The authors declare that they have no known competing financial interests or personal relationships that could have appeared to influence the work reported in this paper.

Acknowledgement

This project has received funding from the European Union's Horizon 2020 research and innovation programme under grant agreement No 957739.

References

- [1] https://ec.europa.eu/energy/sites/ener/files/documents/batteries_europe_strategic_research_agenda_december_2020_1.pdf (accessed: 2022.06.19)
- [2] World Economic Forum, M. analysis. A Vision for a Sustainable Battery Value Chain in 2030 Unlocking the Full Potential to Power Sustainable Development and Climate Change Mitigation. http://www3.weforum.org/docs/WEF_A_Vision_for_a_Sustainable_Battery_Value_Chain_in_2030_Report.pdf (2019) (accessed: 2021.07.19)
- [3] https://ec.europa.eu/commission/presscorner/detail/en/ip_21_3541 (accessed: 2022.06.19)
- [4] https://ec.europa.eu/eurostat/statistics-explained/index.php?title=Renewable_energy_statistics#of_renewable_energy_used_in_transport_activities_in_2019 (accessed: 2022.06.19)
- [5] S. Balischewski, I. Hauer, M. Wolter, C. Wenge, P. Lombardi and P. Komarnicki, "Battery storage services that minimize wind farm operating costs: A case study," *2017 IEEE PES Innovative Smart Grid Technologies Conference Europe (ISGT-Europe)*, 2017, pp. 1-6, doi: 10.1109/ISGTEurope.2017.8260130.
- [6] M. Roos and B. Holthuizen: Congestion of LV Distribution Networks by Household Battery Energy Storage Systems utilized for FCR, aFRR and Market Trading. 53rd International Universities Power Engineering Conference (UPEC). pp. 1-6. 2018. doi: 10.1109/UPEC.2018.8541879.
- [7] Y. Hu, M. Armada, M. J. Sanchez: Potential utilization of battery energy storage systems (BESS) in the major European electricity markets. *Applied Energy*. Vol. 322. 119512. 2022. <https://doi.org/10.1016/j.apenergy.2022.119512>
- [8] F. Dominguez, G. Willegheems, H. Gerard, A. Tzoumpas, K. Drivakou, J. Villar, C. Augusto J. M. Cruz, C. Damas, C. Dikaiakos S. Gandhi: A set of standardised products for system services in the TSODSO-consumer value chain. 2021. <https://onenet-project.eu/wp-content/uploads/2021/08/D22-A-set-of-standardised-products-for-system-services-in-the-TSO-DSO-consumer-value-chain-1.pdf> (Accessed: 2022.10.11)
- [9] A. Wang, S. Kadam, H. Li, S. Shi, Y. Qui: Review on modeling of the anode solid electrolyte interphase (SEI) for lithium-ion batteries. *npj Comput Mater* 4.15 (2018). <https://doi.org/10.1038/s41524-018-0064-0>
- [10] D. Anseán, M. Dubarry, A. Devie, B. Y. Liaw, V .M. García, J. C. Viera, M. González: Operando lithium plating quantification and early detection of a commercial LiFePO₄ cell cycled under dynamic driving schedule. *Journal of Power Sources* vol. 356. pp. 36-46. 2017.
- [11] M. Broussely, Ph. Biensan, F. Bonhomme, Ph. Blanchard, S. Herreyre, K. Nechev, R.J. Staniewicz: Main aging mechanisms in Li ion batteries. *Journal of Power Sources* vol. 146 pp. 90–96. 2005.
- [12] <http://www.molicel.com/wp-content/uploads/INR18650M35A-V2-80096.pdf> (accessed 2022.06.19)
- [13] http://samsungsdi.com/upload/ess_brochure/SamsungSDI_ESS_EN.pdf (accessed 2022.06.19)
- [14] [http://www.dcmx.com.tw/LF280\(3.2V280Ah\).pdf](http://www.dcmx.com.tw/LF280(3.2V280Ah).pdf) (accessed 2022.06.19)
- [15] M. Dubarry, B. Y. Liawa, M.-S. Chen, S.-S Chyan, K.-C. Han, W.-T. Sie, S.-H. Wu: Identifying battery aging mechanisms in large format Li ion cells. *Journal of Power Sources* vol. 196 pp. 3420–3425. 2011.
- [16] F. Leng, C. Tan, M. Pecht: Effect of Temperature on the Aging rate of Li Ion Battery Operating above Room Temperature. *Sci Rep* 5, 12967 (2015). <https://doi.org/10.1038/srep12967>

- [17] L. Zhang, J. Liu, L. Du, P. Fan, X. Xu, Y. Ma, P. Zuo, B. Qu, G. Yin, Q. Fu: LiNi_{0.5}Co_{0.2}Mn_{0.3}O₂/graphite batteries storing at high temperature: Capacity fading and raveling of aging mechanisms. *Journal of Power Sources* vol. 496, 229858. 2021.
- [18] D. Li, H. Li, D. Danilov, L. Gao, J. Zhou, R.-A. Eichel, Y. Yanga, P. H. L. Notten: Temperature-dependent cycling performance and ageing mechanisms of C₆/LiNi_{1/3}Mn_{1/3}Co_{1/3}O₂ batteries. *Journal of Power Sources* vol. 396 pp. 444–452. 2018.
- [19] J. A. Gilbert, J. Barenó, T. Spil, S. E. Trask, D. J. Miller, B. J. Polzin, A. N. Jansen, D. P. Abraham: Cycling Behavior of NCM523/Graphite Lithium-Ion Cells in the 3–4.4 V Range: Diagnostic Studies of Full Cells and Harvested Electrodes. *Journal of The Electrochemical Society* vol. 164, A6054-A6065. 2017.
- [20] I. Buchberger, S. Seidlmayer, A. Pokharel, M. Piana, J. Hattendorff, P. Kudejova, R. Gilles, H. A. Gasteiger: Aging Analysis of Graphite/LiNi_{1/3}Mn_{1/3}Co_{1/3}O₂ Cells Using XRD, PGAA, and AC Impedance. *Journal of The Electrochemical Society*. vol. 162 A2737-A2746. 2015
- [21] B. Ziv, V. Borgel, D. Aurbach, J.-H. Kim, X. Xiao, and B. R. Powell: Investigation of the Reasons for Capacity Fading in Li-Ion Battery Cells. *Journal of The Electrochemical Society*, vol. 161 A1672-A1680. 2014.
- [22] T. Waldmann, M. Wilka, M. Kasper, M. Fleischhammer, M. Wohlfahrt-Mehrens: Temperature dependent ageing mechanisms in Lithium-ion: batteries e A Post-Mortem study. *Journal of Power Sources* vol. 262. pp. 129 – 135. 2014.
- [23] R. Genieser, S. Ferrari, M. Loveridge, S. D. Beattie, R. Beanland, H. Amari, G. West, R. Bhagat: Lithium ion batteries (NMC/graphite) cycling at 80 °C: Different electrolytes and related degradation mechanism. *Journal of Power Sources* Vol. 373. pp. 172 -193. 2018.
- [24] Y. Chen, Y. Kang, Y. Zhao, L. Wang J. Liu, Y. Li, Z. Liang, X. He, X. Lie, N. Tavajohi, B. Li: A review of lithium-ion battery safety concerns: The issues, strategies, and testing standards. *Journal of Energy Chemistry* Vol. 59. pp. 83 – 99. 2021.
- [25] X. Wu, K. Song, X. Zhang, N. Hu, L. Li, W. Li, L. Zhang, H. Zhang: Safety Issues in Lithium Ion Batteries: Materials and Cell Design. *Frontiers in Energy Research* Vol. 7. 2019. <https://doi.org/10.3389/fenrg.2019.00065>
- [26] K. Jalkanen, J. Karppinen, L. Skogström, T. Laurila, M. Nisula, K. Vuorilehto: Cycle aging of commercial NMC/graphite pouch cells at different temperatures. *Applied Energy* vol. pp. 160 - 172. 2015.
- [27] W. Wu, R. Ma, J. Liu, M. Liu, W. Wang, Q. Wang: Impact of low temperature and charge profile on the aging of lithium-ion battery: Non-invasive and post-mortem analysis. *International Journal of Heat and Mass Transfer* vol. 170. 2021.
- [28] B. P. Matadi, S. Geniès, A. Delaille, C. Chabrol, E. de Vito, M. Bardet, J.-F. Martin, L. Daniel, Y. Bulte: Irreversible Capacity Loss of Li-Ion Batteries Cycled at Low Temperature Due to an Untypical Layer Hindering Li Diffusion into Graphite Electrode. *Journal of The Electrochemical Society*, vol. 164. 2017.
- [29] A. Friesen F. Horsthemke, X. Mönnighoff, G. Bruncklaus, R. Krafft, M. Börner T. Risthaus, M. Winter, F. M. Schappacher: Impact of cycling at low temperatures on the safety behavior of 18650-type lithium ion cells: Combined study of mechanical and thermal abuse testing accompanied by post-mortem analysis. *Journal of Power Sources*, vol. 334, pp. 1 – 11. 2016. <https://doi.org/10.1016/j.jpowsour.2016.09.120>
- [30] Y. Li, K. Q. Yan-Bing, H. Yusuf, V. Kaneti, D. Liu, D. L., H. Li, B. Li, F. Kang: Study on the reversible capacity loss of layered oxide cathode during low-temperature operation. *Journal of Power Sources* vol. 342. pp. 24 – 30. 2017. <https://doi.org/10.1016/j.jpowsour.2016.12.033>
- [31] Y. Wu, P. Keil, S. F. Schuster, A. Jossen: Impact of Temperature and Discharge Rate on the Aging of a LiCoO₂/LiNi_{0.8}Co_{0.15}Al_{0.05}O₂ Lithium-Ion Pouch Cell. *Journal of The Electrochemical Society* vol. 164. 2017.

- [32] H. Rubenbauer, S. Henninger: Definitions and reference values for battery systems in electrical power. *Journal of Energy Storage* vol. 12 pp. 87–107. 2017. <http://dx.doi.org/10.1016/j.est.2017.04.004>
- [33] P. Spagnol, S. Onori, N. Madella, Y. Guezennec, J. Neal: Aging and Characterization of Li-Ion Batteries in a HEV Application for Lifetime Estimation. 6th IFAC Symposium Advances in Automotive Control Munich, Germany, July 12-14, 2010.
- [34] S. Saxena, Y. Xing, D. Kwon, M. Pecht: Accelerated degradation model for C-rate loading of lithium-ion batteries. *International Journal of Electrical Power & Energy Systems* vol. 107, pp. 438-445. 2019. <https://doi.org/10.1016/j.ijepes.2018.12.016>.
- [35] G. Ning, B. Haran, B. N. Popov: Capacity fade study of lithium-ion batteries cycled at high discharge rates. *Journal of Power Sources* vol. 117 pp. 160–169. 2003.
- [36] K. Murashko, D. Li, D. L. Danilov, P. H. L. Notten, J. Pyrhonen, J. Jokiniemi: Determination of Li-ion battery degradation mechanisms at high C-rate charging. 2019 IEEE Vehicle Power and Propulsion Conference (VPPC) pp. 1-6. 2019. doi: 10.1109/VPPC46532.2019.8952302
- [37] S. S. Choi, H. S. Lim: Factors that affect cycle-life and possible degradation mechanisms of a Li-ion cell based on LiCoO₂. *Journal of Power Sources* vol. 111 pp. 130–136. 2002. [https://doi.org/10.1016/S0378-7753\(02\)00305-1](https://doi.org/10.1016/S0378-7753(02)00305-1)
- [38] A. Maheshwari, N. G. Paterakis, M. Santarelli, M. Gibescu: Optimizing the operation of energy storage using a non-linear lithium-ion battery degradation model. *Applied Energy* vol. 261 114360. 2020. <https://doi.org/10.1016/j.apenergy.2019.114360>
- [39] P. Svens, M. Behm, G. Lindbergh: Lithium-Ion Battery Cell Cycling and Usage Analysis in a Heavy-Duty Truck Field Study. *Energies* vol 8. pp. 4513-4528. 2015. doi:10.3390/en8054513
- [40] M. Ecker, N. Nieto, S. Käbitz, J. Schmalstie, H. Blanke, A. Warnecke, D. U. Sauer: Calendar and cycle life study of Li(NiMnCo)O₂-based 18650 lithium-ion batteries. *Journal of Power Sources* vol. 248 pp. 839-851. 2014. <http://dx.doi.org/10.1016/j.jpowsour.2013.09.143>
- [41] J. E. Harlow, X. Ma, J. Li, E. Logan, Y. Liu, N. Zhang, L. Ma, S. L. Glazier, M. M. E. Cormier, M. Genovese, S. Buteau, A. Cameron, J. E. Stark, J. R. Dahn: A Wide Range of Testing Results on an Excellent Lithium-Ion Cell Chemistry to be used as Benchmarks for New Battery Technologies. *Journal of The Electrochemical Society* vol. 166 (13) pp. A3031-A3044. 2019. doi: 10.1149/2.0981913jes
- [42] M. Müllera, L. Viernstein, C. N. Truong, A. Eiting, H. C. Hesse, R. Witzmann, A. Jossen: Evaluation of grid-level adaptability for stationary battery energy storage system applications in Europe. *Journal of Energy Storage*, vol. 9. pp. 1–11. 2017.
- [43] Y. Yoo, G. Jang, S. Jung: A Study on Sizing of Substation for PV With Optimized Operation of BESS. *Energy Storage for Energy System Applications*, Vol 8. 2020. doi: 10.1109/ACCESS.2020.3040646
- [44] V. Knap, S. K. Chaudhary, D. -I. Stroe, M. Swierczynski, B. -I. Craciun and R. Teodorescu: Sizing of an Energy Storage System for Grid Inertial Response and Primary Frequency Reserve. *IEEE Transactions on Power Systems*, vol. 31, no. 5, pp. 3447-3456. 2016. doi: 10.1109/TPWRS.2015.2503565.
- [45] Y. Yoo, S. Jung, and G. Jang: Dynamic Inertia Response Support by Energy Storage System with Renewable Energy Integration Substation. *Journal of Modern Power Systems and Clean Energy*, Vol. 8. pp. 260 – 266. 2020.
- [46] M. Farsadi, T. Sattarpour and A. Y. Nejadi: Optimal placement and operation of BESS in a distribution network considering the net present value of energy losses cost. 2015 9th International Conference on Electrical and Electronics Engineering (ELECO), pp. 434-439. 2015. doi: 10.1109/ELECO.2015.7394582.
- [47] S. Jinlei, P. Lei, L. Ruihang, M. Qian, T. Chuanyu and W. Tianru: Economic Operation Optimization for 2nd Use Batteries in Battery Energy Storage Systems. *IEEE Access*, vol. 7, pp. 41852-41859. 2019. doi: 10.1109/ACCESS.2019.2902402.

- [48] S. Zhang, H. Liu, F. Wang, T. Yan, K. Wang: Secondary frequency control strategy for BESS considering their degree of participation. 7th International Conference on Power and Energy Systems Engineering (CPESE 2020). 2020. <https://doi.org/10.1016/j.egy.2020.11.183>
- [49] S. Li, Q. Xu, Y. Xi, K. Hu: Comprehensive setting and optimization of Dead-Band for BESS participate in power grid primary frequency regulation. International Journal of Electrical Power & Energy Systems Vol. 141. 108195. 2022. <https://doi.org/10.1016/j.ijepes.2022.108195>.
- [50] Zhang, H. Liu, F. Wang, Y. Miao J. Dong: Dual-stage operation strategy of BESS for frequency regulation considering planned peak shaving. 7th International Conference on Power and Energy Systems Engineering (CPESE 2020). 2020. <https://doi.org/10.1016/j.egy.2020.11.206>
- [51] R. Xie, Y. Wang, S. Zhang, B. Lin, Q. Chen, F. Wang X. Wang Y. Chen, B.Xia: BESS frequency regulation strategy on the constraints of planned energy arbitrage using chance-constrained programming. 4th International Conference on Clean Energy and Electrical Systems (CEES 2022). 2022. <https://doi.org/10.1016/j.egy.2022.05.129>
- [52] R. Bubbico, F. D'Annibale, B. Mazzarotta, C. Menale: Thermal Model of Cylindrical Lithium-ion Batteries. Chemical Engineering Transactions vol. 74 pp. 1291 – 1296. 2019.
- [53] C. Lin, C. Cui, X. Xu: Lithium-ion Battery Electro-thermal Model and Its Application in the Numerical Simulation of Short Circuit Experiment. World Electric Vehicle Journal Vol. 6. pp. 0603 – 0610. 2013. ISSN 2032-6653.
- [54] S. Kertész, I. Virág. Automatic balancing of solar power plant with battery-powered energy storage. XXXV. Jubileumi Kandó Konferencia 2019. ISBN 978-963-449-163-7.
- [55] <https://mavir.hu/web/mavir-en/frequency> (accessed 2022.05.22)
- [56] <http://www.mekh.hu/publications> (accessed 2022.05.22)